A new model for fatigue life prediction based on infrared thermography and degradation process for CFRP composite laminates

J. Huang[a,b], M.L. Pastor[a,*], C. Garnier[b], X.J. Gong[a]

[a] Institut Clément Ader (ICA), CNRS UMR 5312, University of Toulouse, UPS, 1 rue Lautréamont, 65016 Tarbes, France
[b] LGP-ENIT-INP, University of Toulouse, 47 Avenue d'Azereix, BP 1629, 65016 Tarbes cedex, France

Keywords:
Fatigue life prediction
InfraRed Thermography (IRT)
Damage accumulation
Stiffness degradation

A B S T R A C T

In this paper, a new fatigue life prediction methodology is proposed by combining stiffness degradation and temperature variation measured by InfraRed Thermographic (IRT) camera. Firstly, the improved thermographic method is used to determine the fatigue limit by using the data of stabilized temperature rising. Following this, a two-parameter model is proposed to characterize the stiffness degradation of CFRP laminates with the increase of cycle numbers. After the calibration parameters and the calculation of the normalized failure threshold stiffness, the whole $S-N$ curve can be obtained in a very short time. The proposed model is applied to both the experimental data of triaxially braided CFRP laminates from literature and those of unidirectional CFRP laminates obtained from our fatigue tests. Results show that predicted $S-N$ curves have a good agreement with traditional tests. The principal interests of this model could be listed as follows: (i) it is a more general criterion applicable to different materials; (ii) it has more physical senses; (iii) it allows the determination of the total S-N curve for composite materials in a short time.

1. Introduction

Carbon Fiber Reinforced Polymer (CFRP) composites are increasingly used to manufacture load-bearing components in aerospace, automotive and marine industries due to their high strength-to-weight ratio and high stiffness-to-weight ratio. Recently, fatigue properties of CFRP received more and more concerns since the strength and stiffness of CFRP structural components degrade severely when subjected to cyclic loading during in-service life, which inevitably affects their safety. Consequently, a growing number of researchers have been working on the fatigue behavior of composites. Generally speaking, fatigue limit and stress-life ($S-N$) curves are mostly used to characterize fatigue properties. Nevertheless, it is well known that even for a metallic material, the measurement of one fatigue limit and $S-N$ curve is time-consuming and costly by conducting traditional fatigue tests. Besides, the fatigue properties of the same material can be different due to various loading frequencies, stress ratios, surface roughness values and manufacturing processes [1–4]. Moreover, CFRP composites are more complicated than metals because of their anisotropy and heterogeneity, their fatigue behavior varies also with the nature of fibers and matrix, the volume fraction of fibers, the fiber/matrix interface quality and wide variety of fiber orientations and stacking sequence, etc. Therefore, rapid evaluation of fatigue behavior for CFRP composites is of great importance, especially for lightweight structural design. In order to achieve this goal, one of the main ideas is to acquire more information about the response of material subjected to cyclic loading in a short time.

A number of Non-Destructive Evaluation (NDE) methods, such as radiography [5–7], acoustic emission [8–11] and infrared thermography [12–17] have been employed to in situ monitor and characterize damage evolution within metals and composites under cyclic loading. Among these methods, infrared thermography is advantageous for its real-time and non-contact measurement during fatigue tests. Thus, this NDE technique has been developed originally by Luong [18,19], Risitano [20,21] and their co-workers as a valid approach to determine fatigue limit and $S-N$ curve for metallic materials in a short time (normally around 10 h). Meanwhile, many other criteria based on thermographic data analysis were proposed to determine $S-N$ curve rapidly [22–28]. However, those criteria, which are developed based on metal alloys, may not be accurate anymore for composite laminates because their damage and failure mechanisms are different and even more complicated. Furthermore, those criteria are almost purely empirical formulas which do not take into account damage accumulation process within materials.

The damage mechanism in composite laminates under cyclic loading has been identified usually including matrix cracking, fiber/

* Corresponding author.
E-mail address: marie-laetitia.pastor@iut-tarbes.fr (M.L. Pastor).

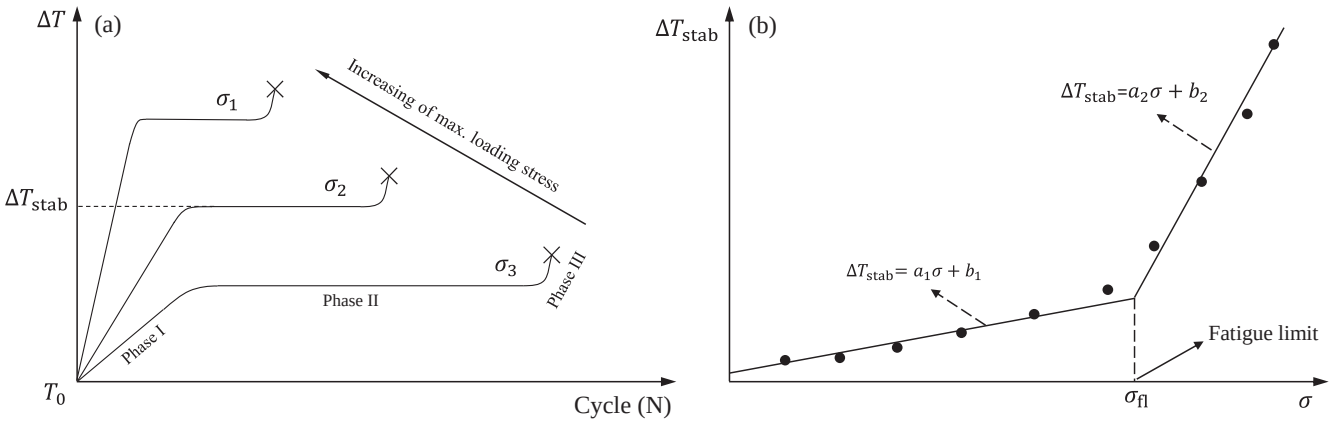

Fig. 1. Rapid determination of fatigue limit based on thermographic data. (a) Typical temperature evolution during fatigue test (T_0: initial temperature; ΔT: temperature rising; ΔT_{stab}: stabilized temperature rising; σ: maximum applied loading stress, $\sigma_1 > \sigma_2 > \sigma_3$). (b) Fatigue limit determined by an improved method based on statistical analysis.

matrix interface cracking, fiber breakage and delamination [29]. According to the literature [30–36], with damage accumulation in laminates, the stiffness and strength degrade obviously. Thus, residual stiffness and strength are frequently used to define damage parameters. Nevertheless, residual strength cannot be evaluated by non-destructive techniques, whereas residual stiffness can be monitored non-destructively and even in real-time during service life [13,37,38]. Therefore, stiffness degradation is a preferable parameter to characterize damage development in a component under cyclic loading. Remarkably, the work of Toubal [12] shows that this damage accumulation process has a strong dependence of the evolution of temperature measured by IRT, so the traditional empirical criteria based on IRT can be explained or even improved by introducing damage accumulation analysis.

In the present paper, a new fatigue life prediction model for composites materials is proposed by combining IRT data and damage accumulation process. Firstly, the improved thermographic method proposed recently [39] is used here to obtain fatigue limit rapidly. Then, a curve fitting method is used to estimate the value of the stiffness threshold under the load corresponding to the fatigue limit. After that, the fatigue damage index of composite materials is established based on stiffness degradation. Following this, a two-parameter model is developed to characterize stiffness degradation as a function of the number of cycles performed under different maximum loading stresses. After parameter calibration with the experimental stiffness degradation and IRT data, the fatigue damage accumulation model is obtained and can be used to predict the $S - N$ curve. Lastly, the experimental data from reference [13] as well as our fatigue testing data of CFRP laminates $[0]_8$ are used to validate the proposed model.

2. Background of IRT technique

Generally, fatigue behavior can be considered as an irreversible process of the degradation of mechanical properties under cyclic loading. There are two main approaches in this irreversible process [19]: (i) a chemical-physical process, such as the movement and the creation of dislocation, chemical bond rupture, creep deformation, etc. (ii) a physical separation of the material, such as cracks, cavitations, etc. Both of those two approaches will cause heat release which is called intrinsic dissipation. By using an infrared thermographic camera, the variation of temperature can be measured with high precision. A local heat conduction equation [40–42] can be employed here to explain the thermodynamic mechanism above:

$$\rho C\dot{T} - \mathrm{div}(k\mathrm{grad}T) = d_i + s_{\mathrm{the}} + s_{\mathrm{ic}} + r_e \tag{1}$$

where ρ, C, T, k are mass density, heat capacity, temperature and heat conduction coefficient, respectively. The first term $\rho C\dot{T}$ on the left side is the heat storage rate due to temperature change, and the second left-hand term $-\mathrm{div}(k\mathrm{grad}T)$ characterizes heat loss rate induced by conduction. The term group on the right side represents the different heat sources: $d_i$denotes the intrinsic dissipation source; s_{the} is the thermoelastic source; s_{ic} describes the heat source induced by the coupling effect between internal variables and temperature; and r_e denotes the external heat supply. When components or specimens are under homogeneous uniaxial loading, we can have the following hypothesis:

(1) Parameters ρ, C, k are material constants and independent of the internal states.
(2) Thermoelastic sources_{the} only causes small fluctuations of temperature but does not contribute to mean temperature rising [39].
(3) Internal coupling source between internal variables and temperature, s_{ic}, can be neglected [43].
(4) External heat supply r_e is time-independent and can be removed by using a reference specimen placed nearby.

Based on the hypothesis above, the intrinsic energy dissipation d_i can be identified as the main contributor to the total heat generated. Particularly, as can be seen from Eq. (1), if d_i remains unchanged, with the increase of temperature, the heat loss rate, $-\mathrm{div}(k\mathrm{grad}T)$, will also increase. It can be deduced that when temperature T reaches a certain value, there exists a balance between heat loss and intrinsic energy dissipation. In this situation, the heat storage rate $\rho C\dot{T}$ equals to zero so that T will remain stable. This conclusion has been proved by a number of experiments (with constant stress ratios) in the previous works [13,20,21,42,44]. As shown in Fig. 1(a), there are three phases from the beginning of the test to the final breakage of the specimen. The temperature increases from an initial value (room temperature) in phase I, then remains stable for the longest period in phase II and finally experiences a sharp increase just prior to the final breakage in phase III. Thus, it can be derived that d_i keeps unchanged in phase II, which indicates that the damage accumulation rate is stable in this phase. If different loading stresses are applied, different stabilized temperature rising ΔT_{stab} will be obtained. Thus, the relationship between ΔT_{stab} and σ can be plotted, as shown in Fig. 1(b). Based on this, two straight lines are used to characterize the relationship and the intersection can be considered as the fatigue limit [18,19].

According to Fig. 1(b), some empirical criteria were proposed to predict fatigue life by establishing a direct relationship between stabilized temperature rising ΔT_{stab} and failure cycle N_f, such as the criterion proposed by Risitano [21]:

$$\Delta T_{stab} N_f = \text{constant} \tag{2}$$

and the criterion proposed by Montesano [13]:

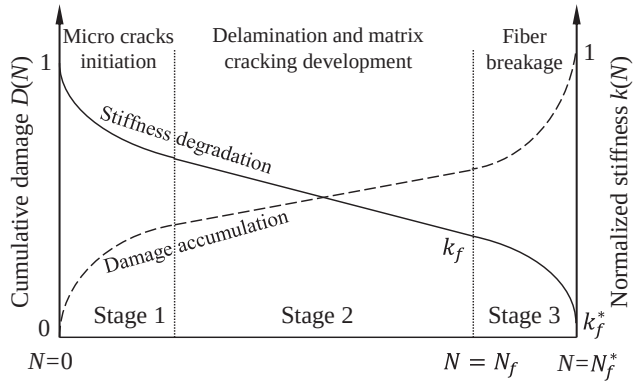

Fig. 2. Typical damage accumulation and stiffness degradation during fatigue tests.

$$\Delta T_{\text{stab}} \log(N_f) = \text{constant} \tag{3}$$

Risitano's criterion was mainly used to determine the whole fatigue *S-N* curves for steels while Montesano's model was proved to be able to predict *S-N* curves for braided CFRP laminates. Thus, it can be known that for different materials, the empirical criteria are not the same. The reason is that those empirical criteria did not take into account the mechanisms of fatigue damage evolution, which could be distinct for different materials. Meanwhile, it is still unknown the correlation between stabilized temperature rising ΔT_{stab} and fatigue damage accumulation speed.

3. Proposed damage accumulation model

3.1. Definition of damage index

It should be noticed that the main damage mechanisms observed in composites laminates under fatigue loading can also be divided into three main stages [29,34], as shown in Fig. 2. In stage 1, the damage zone grows rapidly with micro-cracks initiation in the matrix or/and in the fiber/matrix interface under the first few cycles and some fibers with low strength may break during this stage. Then the damage experiences a slow and steady growth mainly due to delamination and matrix crack propagation in stage 2. Prior to final failure of the specimen, the damage grows dramatically with a mass of fibers breaking in stage 3. It is known that stage 3 is short-period (usually less than 1000 cycles) and unstable so that the first two stages are usually used to estimate the residual life of laminates. Similar to the temperature evolution curves, stage 2 with quasi-stable damage growth rate accounts for the most parts of the total cycle numbers. Therefore, it can be deduced that there is a certain relationship between ΔT_{stab} and the damage accumulation rate. Damage accumulation model based on stiffness degradation [12] is employed in this work and the fatigue damage index is defined as follows:

$$D^*(N) = \frac{K_0 - K(N)}{K_0 - K_f^*} = \frac{1 - k(N)}{1 - k_f^*} \tag{4}$$

where D^* represents cumulative damage level and N is the current number of loading cycles. K_0, $K(N)$ and K_f^* are the stiffness of specimen corresponding to the initial cycle, the N^{th} cycle and the final cycle prior to failure (also called failure threshold stiffness) N_f^*, respectively. $k(N)$, defined as $K(N)/K_0$, is normalized stiffness at N^{th} cycle, and k_f^*, defined as K_f^*/K_0, is normalized failure threshold stiffness at the final cycle. Similar to damage evolution, $k(N)$ also shows three different stages, as shown in Fig. 2.

In order to propose a practical stiffness degradation model, two reasonable simplifications are made here. Firstly, only stage 1 and stage 2 are taken into account because stage 3 is a short period where the damage propagation is unstable and difficult to capture [45,46]. So for conservative consideration, we define N_f as the number of cycle at the end of stage 2 and k_f as the normalized stiffness degradation atN_f (Fig. 2). Secondly, for a given composite laminate with same stacking sequence, geometry and fabrication process, if they are subjected to cyclic loading with fixed loading frequency and loading stress ratio, the critical values of normalized failure threshold stiffness k_f^* can be considered to be independent of the maximum loading stress level, which has been proved by previous experimental work [36]. Thus, the k_f corresponding to the end of stage 2 is supposed to be also independent of the maximum loading stress level. After simplifications, Eq. (5) is obtained based on Eq. (4):

$$D(N) = \frac{1 - k(N)}{1 - k_f} \tag{5}$$

3.2. Proposed model

In order to quantify the damage index, the key is to have the normalized degradation of stiffness as a function of cycle number. As mentioned before, there is a strong relationship between self-heating response and damage evolution. Therefore, in this work, the normalized stiffness degradation is associated with the stable temperature rise as follows:

$$k(N) = 1 - p\Delta T_{\text{stab}} N^{1/q} (q \geq 1) \tag{6}$$

where p and q are two material parameters which are independent of temperature and loading cycles. In Eq. (6), $k(N)$ is dimensionless. In order to keep uniform dimension, the unit of p is in $(^{\circ}\text{C} \times \text{Cycle}^{1/q})^{-1}$ and q is defined as a dimensionless parameter. Those two parameters can be calibrated by experimental data. The term $N^{1/q}$ characterizes the functional form of normalized stiffness degradation with the increase cyclic number during stage 1 and stage 2. The role of parameter q is used to control the shape of the function. ΔT_{stab} varies as a function of the applied maximum stress and it is used to describe the general degradation speed. The role of parameter p is used to regulate the influence ofΔT_{stab}, because the scale of temperature response during fatigue tests depends on the material tested. In the proposed model, the value of normalized stiffness$k(N)$ starts from 1, decreases sharply and then becomes stable when the cyclic number gets large, which is similar as experimental normalized stiffness evolution. By combining Eq. (5) and Eq. (6), the damage index can be expressed as:

$$D(N) = \frac{p\Delta T_{\text{stab}} N^{1/q}}{1 - k_f} (q \geq 1) \tag{7}$$

After calibration with experimental data for a given material, the values of p, q and k_f can be obtained. In fact, ΔT_{stab} can be also considered as a bi-linear function of maximum applied stress σ (see Fig. 1(b)) whose expression is given here:

$$\Delta T_{\text{stab}} = f(\sigma) = \begin{cases} a_1\sigma + b_1 (-b_1/a_1 \leq \sigma < \sigma_{\text{fl}}) \\ a_2\sigma + b_2 (\sigma \geq \sigma_{\text{fl}}) \end{cases} \tag{8}$$

where a_1, b_1, a_2, and b_2 denote four empirical constants determined according to two straight lines in Fig. 1(b) [39]. σ_{fl} is the value of maximum applied loading stress corresponding to fatigue limit [37]. As well known, the damage index has to equal to unity at final or failure cycle N_f: if $D(N_f) = 1$, we have

$$1 = \frac{p\Delta T_{\text{stab}} N_f^{1/q}}{1 - k_f} = \frac{pf(\sigma) N_f^{1/q}}{1 - k_f} (q \geq 1) \tag{9}$$

so the proposed model can predict the whole $S - N$ curve as following:

$$N_f = \left(\frac{1 - k_f}{pf(\sigma)} \right)^q (q \geq 1) \tag{10}$$

3.3. Principal interests of the proposed model

This model has more physical senses. Unlike pure empirical criteria, this model is established based on the analysis of fatigue damage accumulation process in composites. Fatigue damage is caused by matrix cracking, delamination, and fiber breakage, which produce a large amount of heat and lead to temperature variation. Thus, the stabilized temperature rising ΔT_{stab} is considered to be an indicator of the speed of fatigue damage accumulation and the relationship is quantified by Eq. (7).

The model predict *S-N* curve in a short time. To obtain stabilized temperature and stiffness degradation curves, it is not necessary to carry out the fatigue tests until the final failure of the specimen. The proposed model can determine *S-N* curve in 10–12 h, which is significantly less than the time cost by traditional fatigue testing.

The proposed model is more general. The explanation is given as follows: by transforming Eq. (9), we can obtain Eq. (11):

$$\Delta T_{stab} N_f^{1/q} = \frac{1 - k_f}{p} = \text{constant} \tag{11}$$

If $q = 1$, Eq. (11) turns back to Eq. (2) which is the criterion proposed by Risitano. Moreover, if we change the value of q, the results obtained from Eq. (11) can be much closer to those from the criterion proposed by Montesano. An example is given here for explanation. In fact, by similitude of Eqs. (3) and (11), we can just replace the term '$N^{1/q}$' in Eq. (6) with 'log(N)' to obtain the normalized stiffness degradation model based on Montesano's criterion:

$$k(N) = 1 - p' \Delta T_{stab} \log(N) \tag{12}$$

The experimental stiffness degradation data under the maximum loading stress of 65% Ultimate Tension Stress (UTS) in [13] have been used to compare the results of Eqs. (6) and (12), as shown in Fig. 3. It can be seen that the results from the two models have a good concordance. The maximum error of normalized stiffness between two fitted curves is less than 0.19% from 1 to 10^4 cycles. Even if the cycle number is extended to 10^6, the results from the different functions in the two models are always pretty close; the maximum error is less than 4.7%. Therefore, it can be concluded that the proposed model is a more general criterion who can cover both Risitano's criterion and Montesano's criterion.

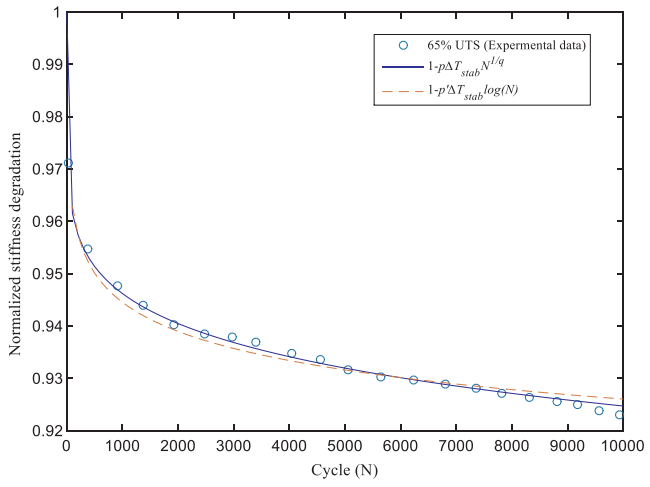

Fig. 3. Comparison of the results of stiffness degradation from Eqs. (6) and (12).

4. Materials and experimental procedure

4.1. Fabrication of specimens

The unidirectional carbon composite specimens used in the present study was fabricated from carbon prepreg composed of the HexPly®M79 matrix (epoxy resin) and the 38% UD150/CHS 12 K high strength carbon fiber. The dimensions of the specimen were as per standard ISO 527-5:2009 [47]. The nominal cure ply thickness was given as 0.13 mm, so 8 plies were used to manufacture the UD composite laminates with 1.04 mm nominal thickness, as shown in Fig. 4. The tabs required for gripping were made from glass fiber fabric prepreg with epoxy resin and the ply orientation angle was given as ± 45°. Autoclave molding process was employed to cure UD composite laminates as well as tabs. The curing of laminates was performed under vacuum (−0.9 bar in the vacuum bag). The curing cycle started with heating up to 80 °C at a heat-up rate of 1 °C/min followed by a 360 min dwell time and then cooled to room temperature at a rate of −1 °C/min. Carbon fiber composite laminate was cut into coupons by using water jet cutting machine and tabs were cut from glass fiber composite laminate by an abrasive cutter. Hysol EA 9394 Part A + B epoxy resin was used for bonding tabs to coupons in an oven at a temperature of 66 °C for more than 24 h.

4.2. Quasi-static tensile testing

Quasi-static tensile testing was conducted until final breakage of the specimen in order to determine the ultimate tensile stress (UTS). Experiments were carried out by using Universal Testing Machine (INSTRON 5500R) with digital image correlation technique (DIC) named 3D system Aramis 2 M (GOM, Braunschweig, Germany). The hardware components of DIC system consists of the following parts: (1) two COMS cameras (1624 * 1236 pixels, 8 bits) for image acquisition, (2) a tripod for support and (3) a computer for software installation. Prior to recording, a layer of white paint was applied to the sample gauge, followed by a layer of finely dispersed black points. According to standard ISO 527–5:2009, three parallel tests were carried out piloted on the displacement and the actual experimental crosshead velocity was set as 2.0 mm min^{-1}. The tensile force was recorded by the sensor of INSTRON 5500R with a scale range of 100 kN and the strain field was calculated from the captured images series by using post-processing software of Aramis. Then the modulus of elasticity was determined, based on the data measured above.

4.3. Fatigue testing with IRT camera

In this study, both the traditional approach and the thermographic approach were used to determine fatigue limit and $S - N$ curve. All uniaxial fatigue tests were conducted under load-control mode at room temperature by using a servo-hydraulic fatigue testing system (INSTRON MODEL 1342). For each load level, the specimens were subjected to a constant loading amplitude sinusoidal wave-form with a frequency of 5 Hz and a stress ratio of 0.1. An infrared camera (Flir Systems SC7000) with InSb sensors, 320 × 256 pixels, and 20 mK thermal sensitivity was employed here to measure the variation of temperature on the surface of specimens in situ and in real-time. The infrared system is composed of the camera connected to a laptop and the software called ALTAIR was used for control, configuration and data post-processing. The detailed experimental setup is shown in Fig. 5(a). A reference specimen was placed nearby the trial specimen in order to monitor the temperature change of ambient temperature. The camera was located in front of specimens at a distance of 660 mm in order to record both reference and trial specimen. The spatial resolution was about 394 × 394 μm^2. The experimental stiffness $K(N)$ was obtained from the N^{th} loop of the measured hysteresis curves by recording the force and the displacement of the clamp (crossbar of the machine),

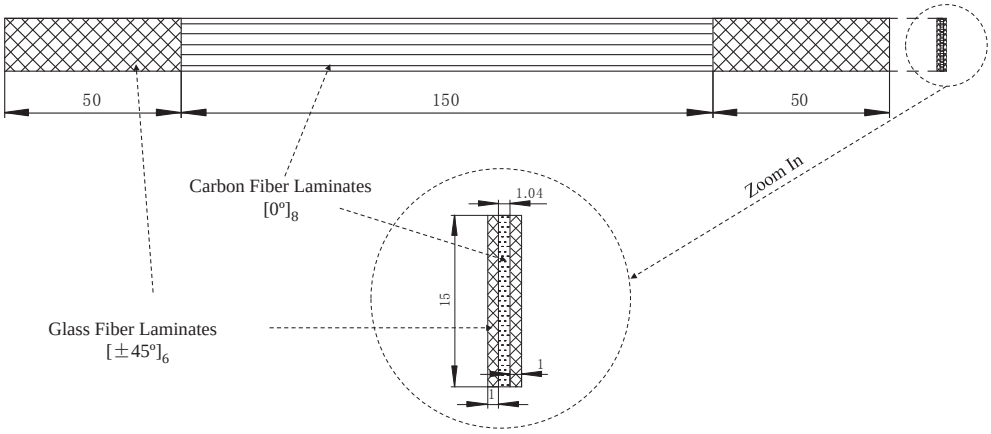

Fig. 4. Dimensions of the specimens used in fatigue loading tests.

as shown in Fig. 5(b). Specifically, $K(N)$ was computed as the slope of the line joining the peak and trough of each cycle of the hysteresis curve. The similar calculation method can be found in [48].

For the traditional fatigue testing approach, several selected maximum stress (95%, 90%, 85%, 80% and 75% UTS) were applied to different tests and each test is conducted in load-control until final failure or over 10^6 loading cycles. Five specimens were tested under each maximum loading stress in order to produce a reliable $S-N$ curve.

For the thermographic testing approach, maximum loading stress level varies from 30% to 90% of UTS at 5% interval in order to obtain the relationship curve between the stabilized rise of temperature and the maximum loading stress. For each maximum loading stress, the specimen was only tested during 6000 loading cycles, which was sufficient for recording the stabilized rise of temperature. A total of three specimens were tested for the thermographic testing approach.

5. Validation of the proposed model

In order to validate the proposed model as well as its application range, two cases are carried out using two types of CFRP composite laminates. For the first case, the proposed model is applied to the experimental data of triaxially braided CFRP laminates presented in [13] while in the second case, our own experimental data of UD CFRP laminates is used.

5.1. Case one: triaxially braided CFRP laminates

The experimental data for triaxially braided CFRP laminates used here have been published in [13], where both thermography and stiffness degradation data are available. The material tested was carbon fiber reinforced composite plate which was made from triaxially braided carbon fiber (T650/35-6 K) fabric with $0^{\circ}/\pm\theta$ braid orientation and thermosetting polyamide resin. The fatigue tests were carried out at a stress ratio of 0.1. In order to show how fatigue limit and $S-N$ curve are clearly determined, the specific procedure and calibration details are shown step by step as follows:

(1) Determine fatigue limit

In this step, the improved thermographic method three in [39] was applied here to determine the fatigue limit (Fig. 6). This method is based on statistical analysis and proved to be an efficient method to determine the fatigue limit with uniqueness. Fig. 6(a) is a plot of temperature evolution curve under the maximum loading stress from 30% to 85% of UTS at the interval of 5% UTS. Fig. 6(b) shows the stabilized temperature rising and the fatigue limit determined is at 67.3% UTS based on Fig. 6(a). Since the data are taken from the reference, we cannot carry out experiments to determine ΔT_{stab_fl}. So for this case, the temperature rising of the intersection is taken as ΔT_{stab_fl}. As shown in Fig. 6, ΔT_{stab_fl} is determined as 6.3 °C.

(2) Determine the values of parameters p and q

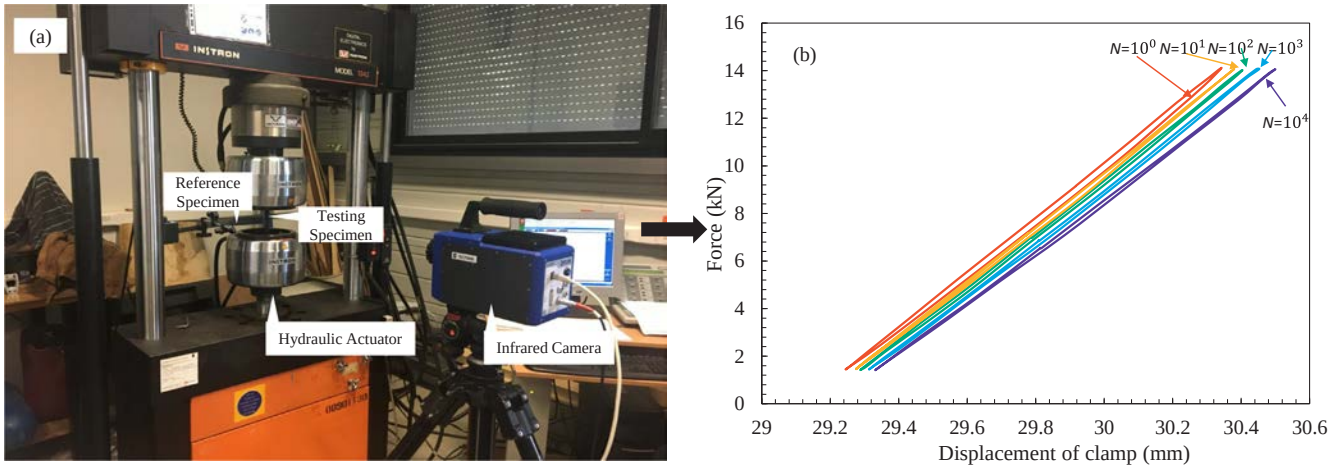

Fig. 5. (a) Experimental setup with infrared camera; (b) Typical hysteresis loops during fatigue tests of UD CRFP laminates.

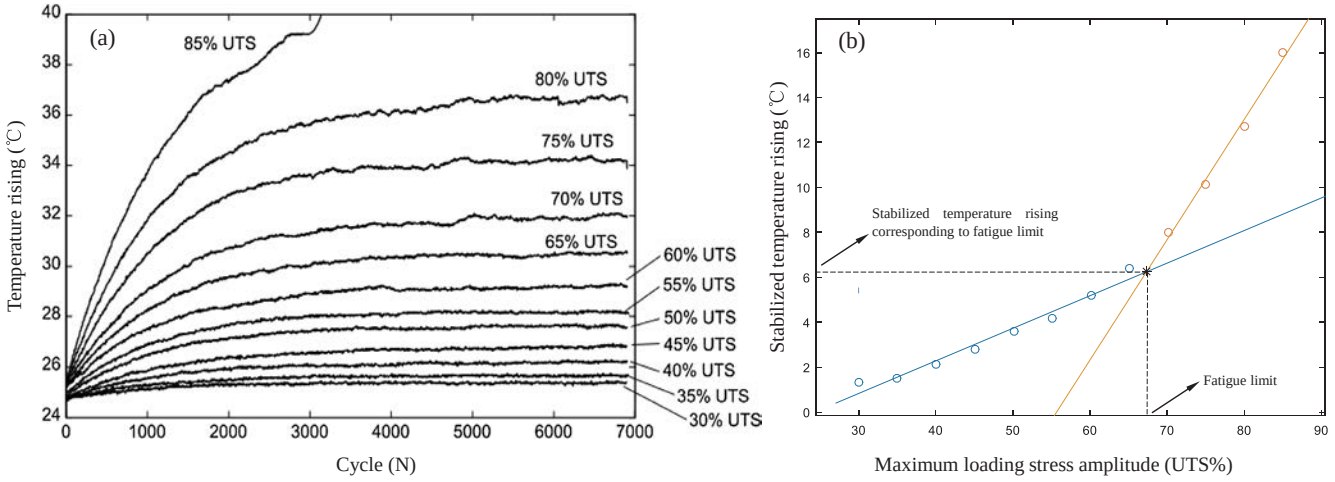

Fig. 6. Experimental data from [13]. (a) Temperature evolution curves; (b) Fatigue limit determination.

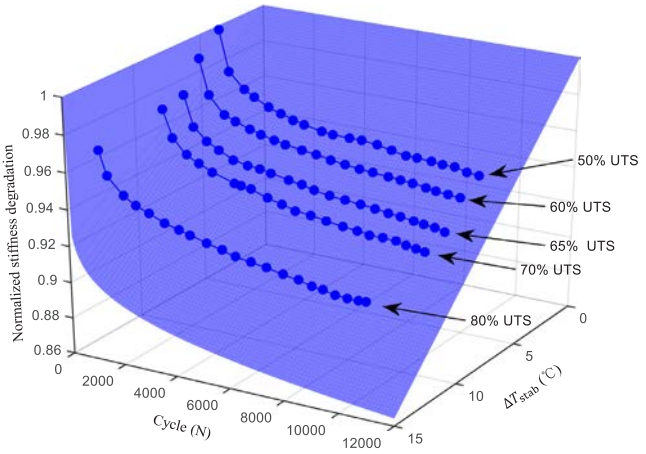

Fig. 7. Surface fitting of Eq. (3) by MATLAB for triaxially braided CFRP laminates.

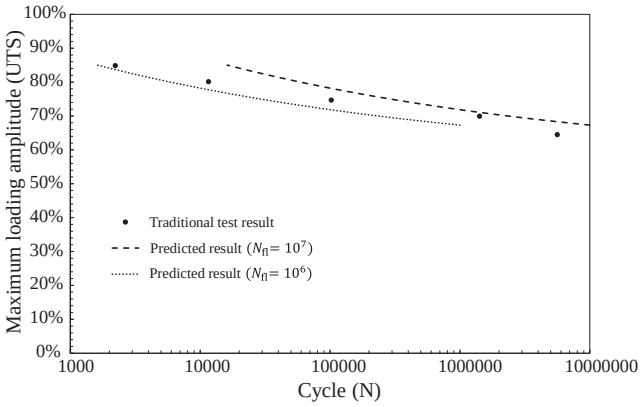

Fig. 8. Comparison of predicted S-N curves and traditional test results [13] for triaxially braided CFRP laminates.

As mentioned in Section 2, only the first two stages are taken into account. According to the data from the experiments in [13], there are five different stiffness degradation curves available and only two parameters are necessary. Thus, for each curve, 20 points were sampled, so a total of 100 points are used for fitting. Herein, Eq. (3) is used to fit the data (3D surface fitting in MATLAB Toolbox) and the values of parameters p and q can be calibrated. As shown in Fig. 7, the translucent surface is the result of surface fitting by Eq. (3) using MATLAB, and the values of p and q are determined at 2.42×10^{-3} ($°C \times Cycle^{1/q}$)$^{-1}$ and 6.85, respectively.

(3) Calculate the failure threshold stiffness

The failure cycle number N_{fl} corresponding to fatigue limit is usually taken between 10^6 and 10^7 [13,41]. Herein, both the $k(N_{fl} = 10^6)$ and k $(N_{fl} = 10^7)$ are considered to calculate the failure threshold stiffness k_f. According to Eq. (3), for $N_{fl} = 10^6$, k_f= 0.886 is obtained while for $N_{fl} = 10^7$, k_f= 0.841.

(4) Calculate the $S - N$ curve

After knowing the values of p, q, and k_f, the whole $S - N$ curve can be plotted according to Eq. (6), and the result is shown in Fig. 8. Traditional test results are also plotted in the same figure for comparison (Fig. 8). However, since the experimental data in [13] is limited, the 95% confidence intervals cannot be given.

For triaxially braided CFRP laminates, the predicted $S - N$ curve corresponding to $N_{fl} = 10^7$ is overall higher than the experimental curve and the error between predict value and experimental is relatively larger for low fatigue life (less than 10,000 cycles). On the contrary, the predicted $S - N$ curve corresponding to $N_{fl} = 10^6$ is lower than the traditional test result. Therefore, due to safety reasons, $N_{fl} = 10^6$ is also recommended here for engineering applications because the predicted result is more conservative.

5.2. Case two: UD CFRP laminates

The ultimate tensile strength (UTS) and Young's modulus (E) of the UD CFRP laminates have been measured by carrying out quasi-static tensile tests with the results of 1487.8 ± 53.2 MPa and 122.6 ± 4.8 GPa, respectively. As mentioned above, the traditional fatigue tests were performed at least on five specimens at each maximum applied stress, which varied from 75% to 95% UTS with an interval of 5% UTS. The fatigue life values N_f corresponding to each maximum applied stress were measured so as to establish the $S - N$ curve presented in Fig. 9. The plot is linear on the log-scale from 10^2 cycles to 10^6 cycles. The data show that the fatigue limit (corresponding to 10^6) of the UD composite laminates is in the range of approximately 75–80% UTS and the specific value is estimated to be 75.8% UTS by using the trend line. For the tests that cycled below fatigue limit, there were no failure specimens after a run-off of 10^6 cycles.

Using the same procedure than the case one, the parameter calibration steps and the results obtained are listed as below:

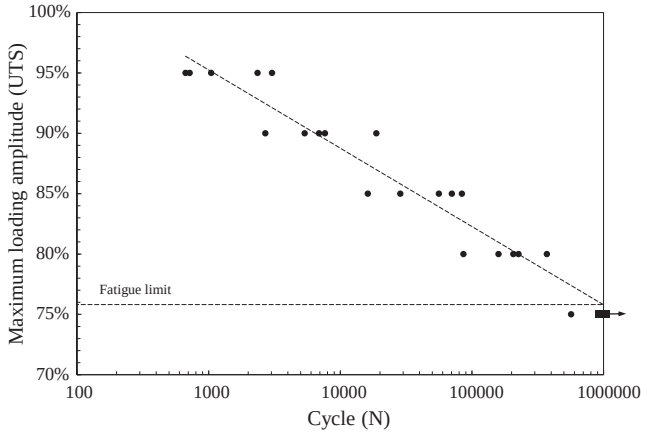

Fig. 9. $S-N$ curve determined by traditional fatigue test (R = 0.1 and f = 5 Hz) of UD CFRP laminates.

(1) Determine fatigue limit based on thermographic data

Fig. 10(a) is a plot of the average surface temperature in gauge section obtained using the IRT camera versus the number of loading cycles for one tested specimen. The maximum stress magnitude is illustrated in the plot at the end of each curve. As can be seen in Fig. 10(a), the temperature profile reached a stabilized plateau at each maximum loading stress from 30% to 90% of UTS. It should be noticed that the plateau section for 90% UTS is very short because of the plateau section is near to Phase III (see Figs. 1 and 2), which is prior to failure. Fig. 10(b) shows the stabilized temperature rising as a function of maximum relative load, based on which the fatigue limit can be determined according to the method described in Section 2. Similarly, the improved two-curve method [39] is firstly applied here and the fatigue limit was determined at 73.8% UTS, which is near to the value (75.8% UTS) determined by traditional tests. Even though the corresponding stabilized temperature rising (ΔT_{stab_fl}) could be determined by intersection point as shown in Fig. 10(b), the measured value is preferable to guarantee the quality of the model. Therefore, we have performed additional fatigue tests under maximum stress equal to the measured fatigue limit stress: 73.8% UTS, the stabilized temperature rising corresponding to fatigue limit (ΔT_{stab_fl}) was so measured as 0.88 °C (± 0.12 °C).

(2) Calibrate the values of parameters p and q

Fig. 11 shows the normalized stiffness degradation of tested specimens as a function of cycle number and stabilized temperature rising for the maximum loading stresses of 50%, 60%, 70%, 75% and 80% of UTS. These five maximum loading stresses were chosen because of the following reasons: (1) the difference among temperature rising curves for maximum loading stress from 30% to 55% UTS is not great, so only 50% UTS was chosen; (2) 10,000 cycles are needed without reaching an unstable period (phase 3); (3) the chosen maximum loading stresses are preferred to be consistent with case one. Similarly, for each curve, 20 points were sampled and 100 points are used for fitting. Eq. (3) is also used to fit the data (3D surface fitting in MATLAB Toolbox) and the values of parameters p and q can be calibrated. The translucent surface is the result of surface fitting by Eq. (3) using MATLAB, which is shown in Fig. 11. And the values of p and q are determined as 1.87×10^{-2} (°C × Cycle$^{1/q}$)$^{-1}$ and 4.75, respectively.

(3) Predict the failure threshold stiffness

Similar as previous case, both the $k(N_{fl} = 10^6)$ and $k(N_{fl} = 10^7)$ are considered to calculate the failure threshold stiffness k_f. According to Eq. (3), for $N_{fl} = 10^6$, k_f= 0.698 is obtained while for $N_{fl} = 10^7$, k_f= 0.509.

(4) Calculate the $S-N$ curve

After knowing the values of p, q, andk_f, the whole $S-N$ curve can be calculated by Eq. (6) and the results are shown in Fig. 12. Traditional test results with the 95% confidence interval are also plotted in the same figure for comparison.

As can be seen from Fig. 12, for UD CFRP laminates, the predicted $S-N$ curve corresponding to $N_{fl} = 10^7$ matches well with the traditional test result for the low and medium fatigue life, whereas the predicted value for high fatigue life (more than 10,000 cycles) is less than the average value of experimental data. The whole predicted $S-N$ curve is inside the 95% confidence interval. The predicted $S-N$ curve corresponding to $N_{fl} = 10^6$ is relatively conservative comparing to experimental results and the predicted fatigue life is less than the traditional test results overall. For engineering applications, $N_{fl} = 10^6$ is recommended because of safety considerations.

6. Discussions

Based on the study of two cases, it can be found that the predicted $S-N$ curve corresponding to $N_{fl} = 10^6$ is conservative for both two kinds of CFRP laminates while the predicted $S-N$ curve

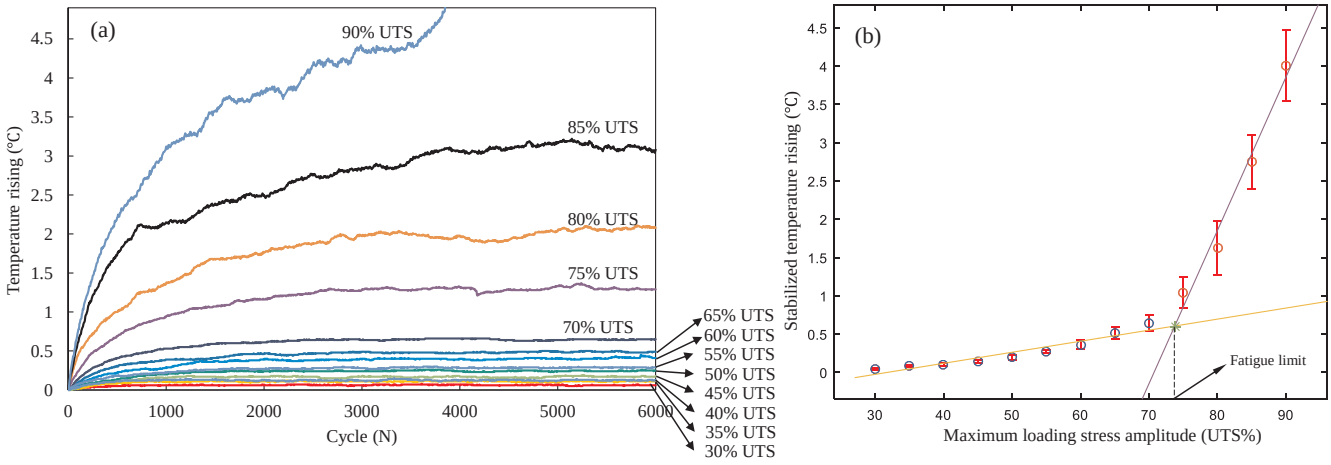

Fig. 10. Fatigue limit determination of UD CFRP based on IRT experimental data. (a) Evolution of the temperature rising as a function of loading cycle number for one specimen; (b) Fatigue limit determined by the improved two-curve method.

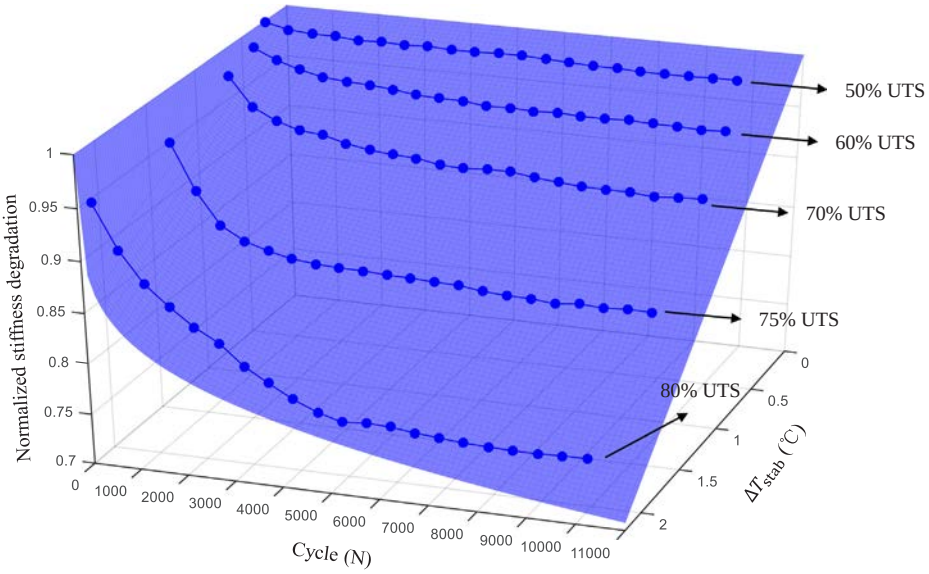

Fig. 11. Surface fitting of Eq. (3) by MATLAB for UD CFRP laminates.

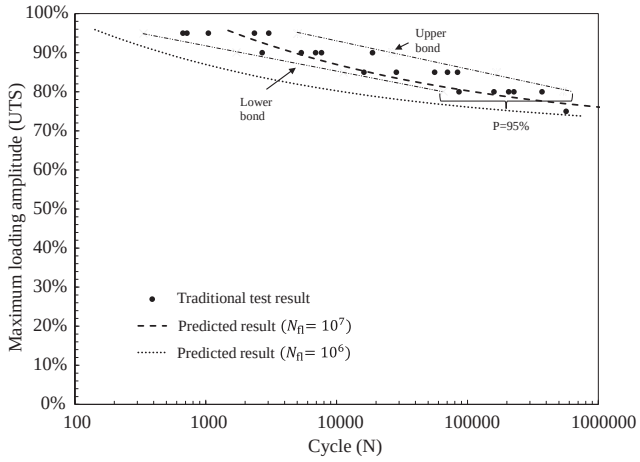

Fig. 12. Comparison of predicted S-N curves and traditional test results for UD CFRP laminates.

corresponding to $N_{fl} = 10^7$ overestimated the fatigue life in some cases. It should be also noticed that under same maximum loading level, the value of ΔT_{stab} of triaxially braided CFRP laminates is much greater than that of UD CFRP laminates. It may be caused by the different dimension of the specimen and different amount of heat generated by internal friction. For thicker and wider specimens, there is more heat generation which may lead to higher temperature rising. Also, the heat generated by internal friction effect between fibers and matrix in UD CFRP laminates could be different. Thus, it is not reasonable to use stabilized temperature rising directly to describe damage evolution. In our proposed model, by adjusting the value of parameter p, the damage accumulation rate related to temperature rising can be regulated. As shown in step two of the parameter calibration procedure, the value of p for UD CFRP laminates is almost 8 times the value of p for triaxially braided CFRP laminates, which indicates that the braided CFRP laminates produce more heat during fatigue tests, compared to UD CFRP laminates. That may be because there is much more friction effect in braided CFRP laminates than in UD CFRP laminates. As for q, the value of parameter q for braided CFRP laminates is greater than UD CFRP laminates, which means that the stiffness degradation of braided CFRP laminates is faster than that of UD CFRP laminates. It is sure that more experimental data are necessary to confirm the physical interpretation of the constants p and q.

7. Conclusions

A practical and quick methodology was proposed to evaluate fatigue life of CFRP laminate in this paper. The damage accumulation process and temperature evolution of composite laminates under fatigue loading were discussed initially to provide theoretical basis. The stabilized temperature rising measured with help of an infrared camera is considered to be able to reflect the rate of damage accumulation. A two–parameter model was developed based on damage accumulation process, which combined stabilized temperature rising and normalized stiffness degradation. It is shown that the proposed model is more general, it can include some empirical criteria proposed in the literature and has a wider application scope. In order to validate proposed methodology, the experimental data obtained on two different types of CFRP laminates, UD and triaxially braided CFRP laminates, were used in the present work to calibrate the two empirical parameters necessary for the establishment of the model. Two failure cycles ($N_{fl} = 10^6$ and $N_{fl} = 10^7$) related to fatigue limit were considered for the determination of the failure threshold stiffness, and then the whole $S - N$ curve corresponding to each failure cycles. Compared to the S-N curve obtained by the traditional testing method, the $S - N$ curve corresponding to $N_{fl} = 10^7$ for UD CFRP laminates is inside the 95% confidence intervals, while the predicted results for triaxially braided CFRP laminates are higher than experimental data. The $S - N$ curve corresponding to $N_{fl} = 10^6$ is recommended for both of the two types of composite materials because the predicted results are relatively more conservative. By comparison of the fatigue life prediction used in the proposed model, the physical sense of each of the two parameters has been discussed. The whole determination process takes about 10–12 h, which is much faster and simpler than traditional fatigue testing method. Therefore, even though the proposed method based on thermographic measurement should have to be confirmed by much more experimental data, it has shown a very promising way to evaluate rapidly fatigue limit and $S - N$ curve for composite laminates, which are considered very important mechanical properties for engineering application of these materials.

Acknowledgements

The author Jia Huang was supported by the China Scholarship

Council for 3 years study at the University of Toulouse.

References

[1] Fargione G, Giudice F, Risitano A. The influence of the load frequency on the high cycle fatigue behaviour. Theor Appl Fract Mech 2017;88:97–106.
[2] Mohammadi B, Fazlali B. Off-axis fatigue behaviour of unidirectional laminates based on a microscale fatigue damage model under different stress ratios. Int J Fatigue 2018;106:11–23.
[3] Lopes HP, Elias CN, Vieira MVB, Vieira VTL, de Souza LC, dos Santos AL. Influence of surface roughness on the fatigue life of nickel-titanium rotary endodontic instruments. J Endod 2016;42(6):965–8.
[4] Bagehorn S, Wehr J, Maier HJ. Application of mechanical surface finishing processes for roughness reduction and fatigue improvement of additively manufactured Ti-6Al-4V parts. Int J Fatigue 2017;102:135–42.
[5] Scott AE, Sinclair I, Spearing SM, Thionnet A, Bunsell AR. Damage accumulation in a carbon/epoxy composite: Comparison between a multiscale model and computed tomography experimental results. Compos A Appl Sci Manuf 2012;43(9):1514–22.
[6] Garcea SC, Mavrogordato MN, Scott AE, Sinclair I, Spearing SM. Fatigue micromechanism characterisation in carbon fibre reinforced polymers using synchrotron radiation computed tomography. Compos Sci Technol 2014;99(Supplement C):23–30.
[7] Garcea SC, Sinclair I, Spearing SM. Fibre failure assessment in carbon fibre reinforced polymers under fatigue loading by synchrotron X-ray computed tomography. Compos Sci Technol 2016;133(Supplement C):157–64.
[8] Masmoudi S, El Mahi A, Turki S. Fatigue behaviour and structural health monitoring by acoustic emission of E-glass/epoxy laminates with piezoelectric implant. Appl Acoust 2016;108:50–8.
[9] Oh KS, Han KS. Fatigue life modeling of short fiber reinforced metal matrix composites using mechanical and acoustic emission responses. J Compos Mater 2013;47(10):1303–10.
[10] Bourchak M, Farrow IR, Bond IP, Rowland CW, Menan F. Acoustic emission energy as a fatigue damage parameter for CFRP composites. Int J Fatigue 2007;29(3):457–70.
[11] Kordatos EZ, Dassios KG, Aggelis DG, Matikas TE. Rapid evaluation of the fatigue limit in composites using infrared lock-in thermography and acoustic emission. Mech Res Commun 2013;54(4):14–20.
[12] Toubal L, Karama M, Lorrain B. Damage evolution and infrared thermography in woven composite laminates under fatigue loading. Int J Fatigue 2006;28(12):1867–72.
[13] Montesano J, Fawaz Z, Bougherara H. Use of infrared thermography to investigate the fatigue behavior of a carbon fiber reinforced polymer composite. Compos Struct 2013;97:76–83.
[14] Palumbo D, De Finis R, Demelio PG, Galietti U. A new rapid thermographic method to assess the fatigue limit in GFRP composites. Compos B Eng 2016;103:60–7.
[15] Crupi V, Guglielmino E, Scappaticci L, Risitano G. Fatigue assessment by energy approach during tensile and fatigue tests on PPGF35. Proc Struct Integrity 2017;3:424–31.
[16] Gao B, He Y, Woo WL, Tian GY, Liu J, Hu Y. Multidimensional tensor-based inductive thermography with multiple physical fields for offshore wind turbine gear inspection. IEEE Trans Ind Electron 2016;63(10):6305–15.
[17] Gao B, Lu P, Woo WL, Tian GY, Zhu Y, Johnston M. Variational bayesian sub-group adaptive sparse component extraction for diagnostic imaging system. IEEE Trans Ind Electron 2018;65(10):8142–52.
[18] Luong MP. Infrared thermographic scanning of fatigue in metals. Nucl Eng Des 1995;158(2):363–76.
[19] Luong MP. Fatigue limit evaluation of metals using an infrared thermographic technique. Mech Mater 1998;28(1):155–63.
[20] La Rosa G, Risitano A. Thermographic methodology for rapid determination of the fatigue limit of materials and mechanical components. Int J Fatigue 2000;22(1):65–73.
[21] Fargione G, Geraci A, La Rosa G, Risitano A. Rapid determination of the fatigue curve by the thermographic method. Int J Fatigue 2002;24(1):11–9.
[22] Huang Y, Li S, Lin S, Shih C. Using the method of infrared sensing for monitoring fatigue process of metals. Materials Evaluation (United States), 42(8); 1984.
[23] Jiang L, Wang H, Liaw P, Brooks C, Klarstrom D. Characterization of the temperature evolution during high-cycle fatigue of the ULTIMET superalloy: experiment and theoretical modeling. Metall Mater Trans A 2001;32(9):2279–96.
[24] Jiang L, Wang H, Liaw P, Brooks C, Chen L, Klarstrom D. Temperature evolution and life prediction in fatigue of superalloys. Metall Mater Trans A 2004;35(3):839–48.
[25] Yang B, Liaw P, Wang G, Morrison M, Liu C, Buchanan R, et al. In-situ thermographic observation of mechanical damage in bulk-metallic glasses during fatigue and tensile experiments. Intermetallics 2004;12(10):1265–74.
[26] Curà F, Curti G, Sesana R. A new iteration method for the thermographic determination of fatigue limit in steels. Int J Fatigue 2005;27(4):453–9.
[27] Amiri M, Khonsari MM. Life prediction of metals undergoing fatigue load based on temperature evolution. Mater Sci Eng, A 2010;527(6):1555–9.
[28] Amiri M, Khonsari MM. Rapid determination of fatigue failure based on temperature evolution: Fully reversed bending load. Int J Fatigue 2010;32(2):382–9.
[29] Vasiukov D, Panier S, Hachemi A. Direct method for life prediction of fibre reinforced polymer composites based on kinematic of damage potential. Int J Fatigue 2015;70:289–96.
[30] Post NL, Lesko JJ, Case SW. 3 - Residual strength fatigue theories for composite materials, fatigue life prediction of composites and composite structures. Woodhead Publishing; 2010. p. 79–101.
[31] Caous D, Bois C, Wahl JC, Palin-Luc T, Valette J. A method to determine composite material residual tensile strength in the fibre direction as a function of the matrix damage state after fatigue loading. Compos Part B: Eng 2017;127(Supplement C):15–25.
[32] Llobet J, Maimí P, Mayugo JA, Essa Y, Martin de la Escalera F. A fatigue damage and residual strength model for unidirectional carbon/epoxy composites under on-axis tension-tension loadings. Int J Fatigue 2017;103(Supplement C):508–15.
[33] Stojković N, Folić R, Pasternak H. Mathematical model for the prediction of strength degradation of composites subjected to constant amplitude fatigue. Int J Fatigue 2017;103(Supplement C):478–87.
[34] Shiri S, Yazdani M, Pourgol-Mohammad M. A fatigue damage accumulation model based on stiffness degradation of composite materials. Mater Des 2015;88:1290–5.
[35] Senthilnathan K, Hiremath CP, Naik NK, Guha A, Tewari A. Microstructural damage dependent stiffness prediction of unidirectional CFRP composite under cyclic loading. Compos Part A: Appl Sci Manuf 2017;100(Supplement C):118–27.
[36] Peng T, Liu Y, Saxena A, Goebel K. In-situ fatigue life prognosis for composite laminates based on stiffness degradation. Compos Struct 2015;132:155–65.
[37] Whitworth HA. A stiffness degradation model for composite laminates under fatigue loading. Compos Struct 1997;40(2):95–101.
[38] Tang R, Guo YJ, Weitsman YJ. An appropriate stiffness degradation parameter to monitor fatigue damage evolution in composites. Int J Fatigue 2004;26(4):421–7.
[39] Huang J, Pastor ML, Garnier C, Gong X. Rapid evaluation of fatigue limit on thermographic data analysis. Int J Fatigue 2017;104(Supplement C):293–301.
[40] Boulanger T, Chrysochoos A, Mabru C, Galtier A. Calorimetric analysis of dissipative and thermoelastic effects associated with the fatigue behavior of steels. Int J Fatigue 2004;26(3):221–9.
[41] Chrysochoos A, Dattoma V, Wattrisse B. Deformation and dissipated energies for high cycle fatigue of 2024–T3 aluminium alloy. Theor Appl Fract Mech 2009;52(2):117–21.
[42] Guo Q, Guo X, Fan J, Syed R, Wu C. An energy method for rapid evaluation of high-cycle fatigue parameters based on intrinsic dissipation. Int J Fatigue 2015;80:136–44.
[43] Guo Q, Guo X. Research on high-cycle fatigue behavior of FV520B stainless steel based on intrinsic dissipation. Mater Des 2016;90(Supplement C):248–55.
[44] Wang XG, Crupi V, Guo XL, Zhao YG. Quantitative thermographic methodology for fatigue assessment and stress measurement. Int J Fatigue 2010;32(12):1970–6.
[45] Tao C, Ji H, Qiu J, Zhang C, Wang Z, Yao W. Characterization of fatigue damages in composite laminates using Lamb wave velocity and prediction of residual life. Compos Struct 2017;166:219–28.
[46] Lee LJ, Fu KE, Yang JN. Prediction of fatigue damage and life for composite laminates under service loading spectra. Compos Sci Technol 1996;56(6):635–48.
[47] ISO 527-5:2009, Plastics - Determination of tensile properties - Part 5: Test conditions for unidirectional fibre-reinforced plastic composites.
[48] Carrillo J, Vargas D, Sánchez M. Stiffness degradation model of thin and lightly reinforced concrete walls for housing. Eng Struct 2018;168:179–90.